Cellulose nanofibrils as a replacement for xanthan gum (XGD) in water based muds (WBMs) to be used in shale formations

Yurany Villada · María Celeste Iglesias · Natalia Casis · Eleonora Erdmann · María Soledad Peresin · Diana Estenoz

Abstract In this work, the potential replacement of xanthan gum (XGD) by cellulose nanofibrils in the composition of water based muds (WBMs) was studied. Bleached (B-CNF) and unbleached (L-CNF) cellulose nanofibrils, mainly differentiated by their lignin content, were tested and their performances were compared with that of XGD. The effects of cellulose nanofibrils on the rheological and filtration properties of WBMs were investigated. Rheometric analysis showed a shear-thinning behavior more noticeable for fluids containing B-CNF and XGD, while filtration properties were improved using L-CNF. The Sisko model was used to determine rheological parameters. Finally, it was found that by replacing XGD by double concentration of L-CNF in a WBM for Argentina shale, similar rheological properties were obtained. Structural changes were assessed by using Scanning Electron Microscopy (SEM). Particles agglomeration and good film formability were observed. Furthermore, WBMs with lignin-containing cellulose nanofibrils exhibited a better thermal stability after aging.

Y. Villada · N. Casis · D. Estenoz (✉)
INTEC (Universidad Nacional del Litoral – Conicet), Güemes 3450, 3000 Santa Fe, Argentina
e-mail: destenoz@santafe-conicet.gov.ar

M. C. Iglesias · M. S. Peresin
Forest Products Development Center, School of Forestry and Wildlife Sciences, Auburn University, 520 Deval Drive, Auburn, AL 36832, USA

E. Erdmann
ITBA (Instituto Tecnológico de Buenos Aires), Av. Madero 399, 1106 Ciudad Autónoma de Buenos Aires, Argentina

Graphical abstract

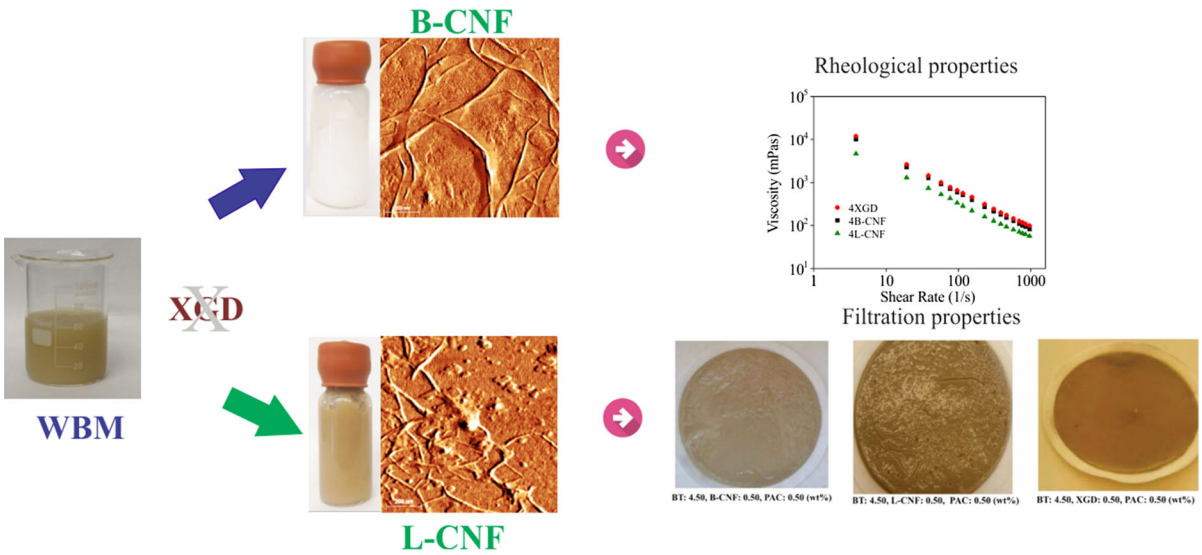

Keywords Lignin · Cellulose nanofibrils · Water based drilling fluid · Xanthan gum · Argentina shale

Abbreviations

A	Cross section area in Eq. (1)
BT	Bentonite
B-CNF	Fully-bleached cellulose nanofibrils
CNF	Cellulose nanofibrils
L-CNF	Lignin-containing cellulose nanofibrils
OBMs	Oil based muds
PAC	Polyanionic cellulose
S-BCNF	Systems of fluids containing BT, B-CNF, PAC and H_2O
S-LCNF	Systems of fluids containing BT, L-CNF, PAC and H_2O
S-XGD	Systems of fluids containing BT, XGD, PAC and H_2O
WBMs	Water based muds
XGD	Xanthan gum
k	Flow consistency coefficient at low shear rate (mPa·s)
K_c	Permeability (mD)
n	Flow behavior index
q	Filtrate rate (cm^3/s)
t_c	Thickness of filter cake (cm)
$\dot{\gamma}$	Shear rate (1/s)
ΔP	Pressure difference (6.80 atm)
η_∞	Viscosity at infinite shear rate (mPa·s)
μ	Viscosity of the filtrate at 25 °C (1.00 cP)

Introduction

Drilling fluids play an important role in oil and gas drilling operations. Cleaning and stabilizing the well, suspending and carrying out cuttings, reducing friction between formation and drilling tools, cooling and lubricating tools, promoting hydraulic power, and being compatible with logging tools are the most important properties of these fluids (Aftab et al. 2017; Khodja et al. 2010a; Mao et al. 2015; Meng et al. 2012). Successful drilling operations are highly dependent on the selection of the desirable characteristics of fluids, which are determined to a large extent by their rheological and fluid filtration properties (Song et al. 2016a). Depending on the composition, fluids are classified in two groups: water-based muds (WBMs) and oil-based muds (OBMs). Between these two, OBMs exhibit high performance regarding penetration rate, clay swelling in the shale, excellent filtration control, wellbore stability, high lubricity, high thermal stability, high salt tolerance, and good ability to transport cuttings (Shah et al. 2010). However, they present some disadvantages related to the environmental impact, cost, and negative effects

on the well cementing due to the poor adhesion between the casing and the formation (Khodja et al. 2010b; Liu et al. 2015; Shah et al. 2010; Zhong et al. 2012).

In recent years, different additives have been used in WBMs to improve their rheological and filtration properties. Among them, natural polymers (starch, isolate soy protein, arabic gum, guar gum, diutam gum, welan gum, xanthan gum-XGD-, polyanionic cellulose-PAC-, tamarind gum, scleroglucan, chitin, and others cellulose derivates) (Caenn and Chillingar 1996; Carico and Bagshaw 1978; Ezell et al. 2010; Gao 2015; Hamed and Belhadri 2009; Iscan and Kok 2007; Jang et al. 2015; Li et al. 2015a, 2018; Mahto and Sharma 2004; Menezes et al. 2010; Navarrete et al. 2000, 2001; Olatunde et al. 2012; Robert and Baker 1974; Villada et al. 2017; Warren et al. 2003) synthetic polymers (polyacrylamide and polyacrylates) (Nunes et al. 2014; Yan et al. 2013), and inorganic nanoparticles (graphene, graphite, nanosilica, carbon nanotube, and metallic oxides) (Barry et al. 2015; Cheraghian et al. 2013; Fazelabdolabadi et al. 2014; Ismail et al. 2016; Kosynkin et al. 2011; Nasser et al. 2013; Sayyadnejad et al. 2008; Sensoy et al. 2009; Sharma et al. 2012) have been extensively investigated. Currently, many studies have been reported on the development of new formulations for high performance WBMs, from environmental, economic, and performance points of view. In this sense, the use of polymers from renewable and biodegradable sources that also exhibit good properties and low cost represent a promising alternative. The potential uses of lignocellulosic sources in the development of novel, high value-added products have generated enormous interest not only in the academic community but also in the industry (Li et al. 2015b; Xu et al. 2013).

Lignocellulosic fibers can be described as natural composite materials where cellulose nanofibrils are linked together mainly with hemicellulose and lignin. Within the structure of the fiber, different regions regarding the organization of the cellulose chains can be found; highly ordered cellulose chains are known as crystalline regions, while disordered cellulose chains mixed with hemicelluloses and lignin are referred to as amorphous or less ordered regions (Panshin and De Zeeuw 1970; Sjöström 1993).

As the main component of lignocellulosic materials (about 45% in wood species), cellulose has been largely used for millennia to supply human necessities (Klemm et al. 2011). Cellulose is a linear homopolymer made-up by β-D-glucopyranose units which are linked by (1–4) glycosidic bonds (O'sullivan 1997; Sjöström 1993). The arrangement of the inter- and intramolecular bonds confers rigidty, stability, and water insolubility to the cellulose fibers (Moon et al. 2011).

As nanotechnology has gained in popularity, lignocellulosic materials have been fractionated to the nanoscale where their components can be separated and utilized in different applications. The nanoscale dimension of cellulose, as well as its morphology, aspect ratio, surface chemistry and surface energy impart very distinctive properties when compared to cellulose fibers, such as improved mechanical performance and thermal stability (Klemm et al. 2005).

Different raw materials and processes to isolate nanocellulose have been widely studied. From lignocellulose materials such as wood, cotton, linen, sugar cane, and agricultural wastes (Herrick et al. 1983; Nakagaito and Yano 2004; Pääkkö et al. 2007; Spence et al. 2011; Turbak et al. 1983) to even bacteria and tunicates (Capadona et al. 2007; Jorfi et al. 2013, Nakagaito et al. 2005; Olsson et al. 2010), nanocellulose has been effectively produced. Sources and choice of processing for nanocellulose production will directly impact specific characteristics, such as morphology, aspect ratio, rheological and optical properties, among others (Klemm et al. 2011; Moon et al. 2011). The three main groups of nanocelluloses are cellulose nanocrystals (CNC), cellulose nanofibrils (CNF), and bacterial nanocellulose (BNC). Although research involving the utilization of BNC is increasing considerably (Hu et al. 2011; Marchetti et al. 2017; Nimeskern et al. 2013; Picheth et al. 2014; Pirich et al. 2015), CNC and CNF production processes and yields have been improved. The most commonly applied method to obtain CNC involves the dissolution of the amorphous region of the elementary fibrils. Thus, nanocrystals of cellulose (also known as whiskers) are usually isolated through mild acid hydrolysis (Postek et al. 2011). After this process, crystals of 10–20 nm in width and several hundred nm in length can be obtained (Xu et al. 2013). CNFs can be produced by mechanical disintegration, or by combining mechanical treatments with enzymatical or chemical pretreatments to reduce the energy consumption of the

process and improve the nanofibril properties (Klemm et al. 2011; Moon et al. 2011; Pääkkö et al. 2007). After the mechanical treatments, cellulose nanofibrils are still constitute by the crystalline and amorphous regions and their diameters are drastically reduced. CNF particles are long, flexible structures with a fibril diameter similar to or greater than that of CNC (Xu et al. 2013) that form strong gels at low solid contents (2 wt%).

Although most of the studies regarding nanocellulose have considered the production of CNF from fully-bleached cellulose fibers (B-CNF), an increasing interest in the utilization of lignin-containing cellulose nanofibrils (L-CNF) has been reported in the last decade (Bian et al. 2017; Diop et al. 2017; Rojo et al. 2015; Solala et al. 2012; Spence et al. 2010a, b). The utilization of unbleached cellulose pulps to produce CNF with residual lignin and hemicelluloses is an interesting alternative due to the ease defibrillation and the fibril properties such as water barrier, thermoplasticity, among others (Ferrer et al. 2012; Nair et al. 2017; Rojo et al. 2015; Wang et al. 2012). From the economical and environmental points of view, the production of L-CNF is attractive, since the lignin removal as well as the following bleaching step that requires chemicals are no longer necessary (Rojo et al. 2015; Spence et al. 2010b).

The distinctive characteristics of nanocelluloses have made them attractive for use in composites, energy storage, packing and coatings, aerogels and hydrogels, biodegradable composites, water remediation, films and coatings, medicine applications, magnetic nanorods, supercapacitors, among others (De France et al. 2017; Du et al. 2017; Hubbe et al. 2017; Kargarzadeh et al. 2017; Li et al. 2015b; Mahfoudhi and Boufi 2017; Ng et al. 2017; Seabra et al. 2018; Voisin et al. 2017). Although several studies have been published on the use of nanocellulose for different applications, there is little research describing the utilization of nanocellulose as an additive in drilling fluids. Li et al. (2015c, d) and Song et al. (2016a,b) investigated the effect of CNC and CNF on the rheological and filtrate properties of aqueous dispersions containing nanocellulose from fully-bleached pulp, bentonite (BT), and PAC. The authors suggested that no publications had appeared on the addition of nanocelluloses from unbleached pulp as additive in WBMs. In addition, no studies on the use of nanocelluloses in WBMs specifically for shale formations had been reported.

In this study, a sustainable alternative for the design of WBMs with environmental and economic advantages for use with shale formations is proposed. In particular, the replacement of XGD, a natural polymer with viscosifying and viscoelastic properties that is stable over a wide range of temperature, salinity and pH, is studied. Due to its chemical structure, low cost and environmentaly friendly characteristics, two kinds of CNFs (bleached and unbleached) are proposed as an alternative for such replacement and their performances in WBMs are evaluated. The effects of WBMs components on their structural, rheological, filtration and thermal properties are investigated. Additionally, rheological properties of WBMs are also theoretically described using the Sisko model, and specific studies on WBMs for Argentina shale formation is presented.

Materials and methods

Preparation

Cellulose nanofibrils

Cellulose pulps, produced by La Montañanesa pulp mill (Torraspapel - Lecta Group, Spain), were supplied for the National Institute of Agricultural and Food Research and Technology (INIA, Spain). Two different cellulose nanofibrils were evaluated; the first sample from a bleached, never dried birch Kraft pulp (B-CNF), and the second sample from unbleached Eucalyptus Globulus pulp (L-CNF). Cellulose nanofibrils were kindly produced at VTT Technical Research Center of Finland Ltd. (Espoo, Finland).

Prior to the nanocellulose production, lignocellulosic pulps were washed using $NaHCO_3$ in order to convert the carboxylic groups of the cellulose fibers into their sodium form. This step has been extensively used to increase the repulsion forces between fibers and allow for easier mechanical defibrillation (Ferrer et al. 2012; Horvath et al. 2006; Lahtinen et al. 2014; Scallan and Grignon 1979).

Concerning the manufacturing method, both cellulose pulps were first diluted at approxymately 1.8% of consistency and then dispersed to avoid the formation of agglomerates. Then, cellulose nanofibrils were obtained by using a Supermasscolloider friction

grinder MKZA10-15 J (Masuko Sangyo Co., Fiber) followed by the utilization of a Microfluidizer M7115-30 (Microfluidics Corporation). By using the Masuko grinder, suspensions were ground when passing between one stationary and one rotating stone which allowed the fibers to be broken and delaminated. Afterwards, suspensions were forced to pass through a small chamber with a specific geometry which allowed the fracture of the fiber into smaller portions. Finally, a gel-like nanocellulose suspension was obtained for both samples (Fig. 1).

Fluids

Different fluids were prepared to evaluate the properties of CNFs in aqueous suspension and to study the CNF performances as additives in WBMs. In the case of WBMs, both simple fluids containing BT, PAC and XGD or CNFs, and complex WBMs formulated for Argentina shale were considered.

Aqueous cellulose nanofibrils suspensions Aqueous suspensions of CNFs (B-CNF or L-CNF) were prepared to determine their rheological properties. CNFs were diluted at 0.5 wt% using deionized water following a ultrasonic treatment for 15 min.

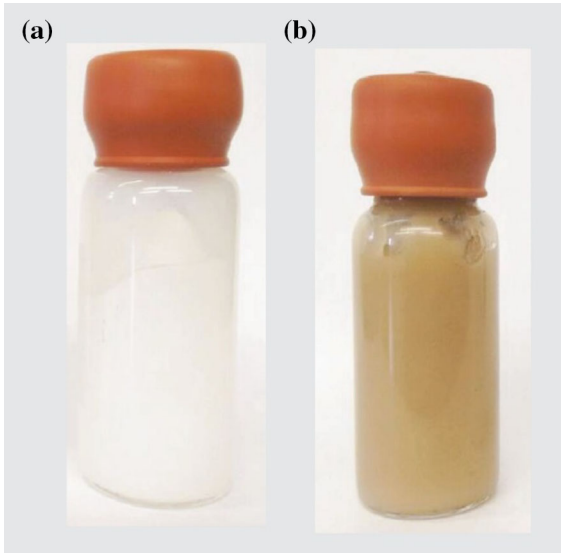

Fig. 1 CNF suspensions: **a** B-CNF from bleached cellulose pulp, and **b** L-CNF from cellulose pulp containing residual lignin

Water-based drilling fluids systems To evaluate possible substitutions of the XGD additive on WBMs, three different systems were studied: S-BCNF (BT/B-CNF/PAC/H_2O), S-LCNF (BT/L-CNF/PAC/H_2O), and S–XGD (BT/XGD/PAC/H_2O). For each system, different fluids were prepared and distinguishabled by the concentrations of CNFs (B-CNF, L-CNF), XGD, BT and PAC (Table 1). The set of compositions were selected on the basis of reported information (Baker Hughes INTEQ 1999; Li et al. 2015c, 2018).

Fluid preparation was made by following the Standard Procedure for Testing Drilling Fluids (API Recommended Practice 13B-1 2003) with a certain order of addition. Briefly, water and bentonite were added to a 500 ml vessel and stirred for 30 min. The suspension was then allowed to stand for 16 h at room temperature. Then, B-CNF, L-CNF or, XGD were added and the mixtures were stirred for 10 min. Finally, PAC was added and the suspension was stirred for 10 min. BT, XGD and PAC additives were provided by service companies of Argentina.

Water-based drilling fluid systems for Argentina shale Special WBMs for Argentina shale containing L-CNF or XGD were prepared following the procedure reported by Villada et al. (2017). Shale characterization was also informed in the cited article. Except for XGD, PAC, and L-CNF, whose concentrations are shown in Table 2, the composition of other additives were taken from Villada et al. (2017).

Characterization

Cellulose nanofibrils

Morphology Atomic force microscopy (AFM) was utilized as a morphological characterization technique. AFM analyses were performed to assess the morphology and roughness of the dispersed CNF using a scanning probe microscope (Agilent model 5400, USA). CNF suspensions at 0.1 wt% were dropped onto silica surfaces (10 mm × 10 mm) and air-dried for a few days. Then, surfaces were mounted onto aluminum sample holders. Scanning was performed in tapping mode, using Bruker AFM probes (model TESPA, doped Si, frequency:

Table 1 Composition of S-BCNF, S-LCNF, and S-XDG systems

S-BCNF systems: BT/B-CNF/PAC/H_2O				S-LCNF systems: BT/L-CNF/PAC/H_2O				S-XGD systems: BT/XGD/PAC/H_2O			
Fluid	BT (wt %)	B-CNF (wt %)	PAC (wt %)	Fluid	BT (wt %)	L-CNF (wt %)	PAC (wt %)	Fluid	BT (wt %)	XGD (wt %)	PAC (wt %)
1B-CNF	0.00	0.50	0.50	1L-CNF	0.00	0.50	0.50	1XGD	0.00	0.50	0.50
2B-CNF	1.00	0.50	0.50	2L-CNF	1.00	0.50	0.50	2XGD	1.00	0.50	0.50
3B-CNF	3.00	0.50	0.50	3L-CNF	3.00	0.50	0.50	3XGD	3.00	0.50	0.50
4B-CNF	4.50	0.50	0.50	4L-CNF	4.50	0.50	0.50	4XGD	4.50	0.50	0.50
5B-CNF	6.00	0.50	0.50	5L-CNF	6.00	0.50	0.50	5XGD	6.00	0.50	0.50
6B-CNF	4.50	0.00	0.50	6L-CNF	4.50	0.00	0.50	6XGD	4.50	0.00	0.50
7B-CNF	4.50	0.10	0.50	7L-CNF	4.50	0.10	0.50	7XGD	4.50	0.10	0.50
8B-CNF	4.50	0.25	0.50	8L-CNF	4.50	0.25	0.50	8XGD	4.50	0.25	0.50
9B-CNF	4.50	0.50	0.00	9L-CNF	4.50	0.50	0.00	9XGD	4.50	0.50	0.00
10B-CNF	4.50	0.50	0.10	10L-CNF	4.50	0.50	0.10	10XGD	4.50	0.50	0.10
11B-CNF	4.50	0.50	0.25	11L-CNF	4.50	0.50	0.25	11XGD	4.50	0.50	0.25

Table 2 L-CNF, XGD and PAC composition of WBM for Argentina shale (composition of other additives as Villada et al. 2017)

Fluid	C_{XGD} (wt %)	C_{PAC} (wt %)	$C_{L\text{-}CNF}$ (wt %)
Base mud	0.15	0.80	–
A	–	0.80	0.15
B	–	0.80	0.30
C	–	0.80	0.45

320 kHz, force constant: 42 N/m). AFM images were further analyzed using Gwyddion software.

Thermal behavior Thermogravimetric analyses (TGA) were performed to determine thermal stability of CNFs. A Q500 thermobalance from TA Instruments was used. The applied heating rate was from 10 °C/min at room temperature up to 800 °C in nitrogen atmosphere (100 ml/min), employing a platinum pan. Sample size was approximately 5 mg. TGA temperature was calibrated with the curie temperature of a standard cooper sample provided by TA Instruments.

Surface charge and Z potential Finally, in order to study the fluid dynamic stability of suspensions, zeta potential and charge densities were measured. Zeta potential measurements were performed at pH 7.00 using a Zetasizer Nano-series Malverl (ZS90). CNF suspensions were previously diluted (0.1 wt%) in deionized water (without salt content) and sonicated for 10 min.

Charge densities of the fibers were measured using a polyelectrolyte titration method. A 450 μN poly (diallyldimethylammonium chloride) (pDADMAC) solution from Sigma-Aldrich with an average molecular weight of 400–500 kDa was used as titrant. This solution was previously validated using 0.001 N potassium polyvinyl sulfate as a standard solution from AppChem Ltd UK (England). Titrations were performed at 0.0001 N NaCl ionic strength and pH 8.4 and using a streaming current detector (Chemtrac CCA 3100).

Fluids

Steady-shear rheological behavior Rheometric properties of fluids were measured using a Brookfield DV3TRV (cone/plate) viscometer. The CP-51Z configuration was used with a shear rate range of 3.84–960 1/s at 25 °C. Prior to each viscosity measurement, the samples were pre-sheared at 960 1/s during 30 s to erase any shear history. Measurements were repeated three times to ensure that the results were reproducible.

Filtration properties To measure filtration properties, a filter press with Whatman filter paper No. 50 was used with CO_2 as pressurizing gas at 6.80 atm. Filtrate readings were performed at 0.16, 5, 7.5, 10, 15, 20, 25 and 30 min at room temperature.

The filtration rate was measured with the liquid flowing through the already assembled cake,

following the method described by Li et al. (2015c). The formation of the filter cakes was carried out according to the API standards (API Recommended Practice 13B-1 2003). Briefly, 100 mL of distilled water were added above each formed cake on the cell of the filter press. Then, the distilled water flowed through the cakes under pressure of 6.80 atm and the volumes of filtrate were measured. Finally, filter cakes were removed and dried at room temperature and their thickness measured using a caliper. The filtration rates were obtained from slope of the fitted straight line of the graphic filtrate volume *vs* time.

The permeability of filter cakes was obtained according to Darcy's law as:

$$K_C = \frac{\mu t_c dv}{\Delta P A dt} = \frac{\mu t_c q}{\Delta P A} \quad (1)$$

where μ is the viscosity of the filtrate at 25 °C (1.00 cP), t_c is the thickness of each filter cake (cm), ΔP is the pressure difference (6.80 atm), A is the cross section area (44.16 cm^2) and q is the filtrate rate (cm^3/s) determined from the liquid flowing through the formed cakes, as it was described before.

Structural The structural characterization of drilling fluids was observed by scanning electron microscopy (SEM) in a JEOL JSM-35C equipped with the image acquisition program JEOL SemAfore. Samples at 0.1 wt% were placed over an aluminum stub, sputter coated with gold under an argon atmosphere (SPI Supplies, 12157-AX) and examined using an acceleration voltage of 20 kV. These analyses were carried out to study morphological and structural changes of drilling fluid by the interaction with the different polymers.

Dynamic-aging test All aging tests were developed using a roller oven, OFITE at 91 °C for 16 h. After aging, the rheometric properties were determined following the same procedure used for fluids before aging.

Theoretical rheological study-Sisko model Sisko rheological model adequately predicts the relationship between the viscosity and the shear rate $\eta : f(\dot{\gamma})$ represent by:

$$\eta = \eta_\infty + k\dot{\gamma}^{n-1} \quad (2)$$

where η_∞(mPa·s) is the viscosity at infinite shear rate, k(mPa·s) is the flow consistency coefficient at low shear rate, $\dot{\gamma}$ (1/s) is the shear rate and n is the flow behavior index.

In order to obtain the corresponding rheological parameters, the model was adjusted to the experimental data.

Results and discussion

Characterization of cellulose nanofibrils

Morphology

Photographs of the CNF suspensions are presented in Fig. 1. As it can be observed, the difference in coloration of both CNF suspensions is due to the presence of residual lignin on L-CNF. B-CNF was obtained from fully bleached cellulose pulp as starting material.

AFM was utilized to investigate the morphology and diameter of the CNF fibrils. Figure 2 shows representative amplitude images obtained using AFM. The mean diameter of fibrils and standard deviations were 15.7 ± 3.1 and 14.8 ± 4.6 nm for samples B-CNF and L-CNF, respectively, as calculated using ImageJ software. These results suggest a reduction of the diameter due to the residual lignin and hemicellulose content in agreement with similar reports (Ferrer et al. 2012; Rojo et al. 2015). Solala et al. (2012) suggested that the presence of lignin induces the stability of the radicals during the mechanical defibrillation, decreasing the attraction between the fibrils and favoring their separation. Consequently, smaller fibril diameters are expected at greater lignin and hemicellulose contents.

Values of root-mean-square (RSM) roughness of 3.33 ± 0.33 nm, and 2.83 ± 0.40 nm were obtained from AFM images for B-CNF and L-CNF, respectively. Roughness is considered an indication of diameter of the fibrils and the degree of consolidation on the surface upon drying. The roughness of L-CNF in comparison with B-CNF suggests smaller widths (Fig. 2b) (Ferrer et al. 2012; Rojo et al. 2015). This observation is consistent with other works that report smaller diameters on nanocellulose obtained from unbleached pulps (Ferrer et al. 2012; Rojo et al. 2015).

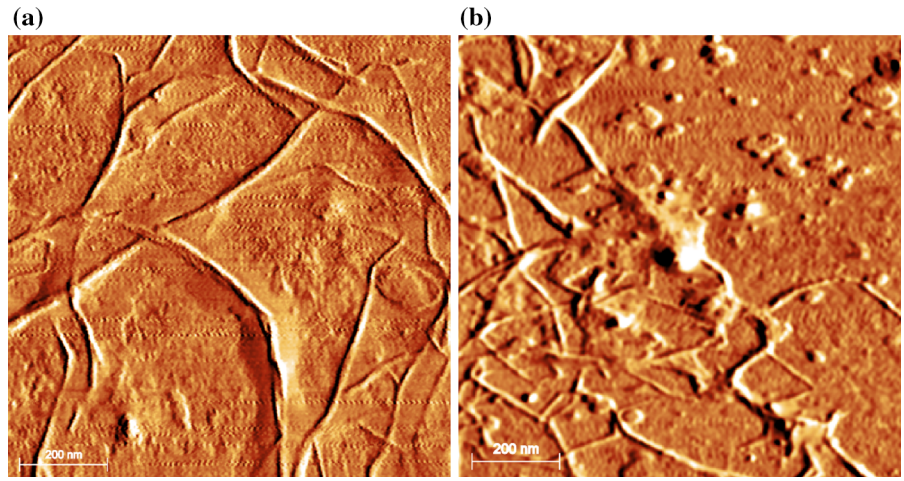

Fig. 2 Amplitude micrographs (1 μm × 1 μm) obtained by AFM: **a** B-CNF and **b** L-CNF

This has been attributed to the ability of lignin to promote fibrillation, based on its ability to scavenge mechanoradicals formed during the fibrillation process (Rojo et al. 2015; Solala et al. 2012). Additionally, the loss of hemicelluloses during delignification influences the fibril size and distribution (Tenhunen et al. 2014).

Table 3 Charge density and zeta potential values of CNFs

Sample	Charge Density (μeq/g)	ζ Potential (mV)
B-CNF	− 50.11 ± 0.51	− 24.70 ± 0.70
L-CNF	− 58.00 ± 0.85	− 34.70 ± 2.40

Surface charge and Z potential

The results of charge density and zeta potential are shown in Table 3. It can be observed that both CNFs present negative surface charges. Lignocellulosic pulps are washed into their sodium form, prior to their fibrillation for nanocellulose production (Ferrer et al. 2012; Horvath et al. 2006). This step increases the repulsion forces between fibers by displacing the COOH ↔ COO– equilibrium towards the right, thus increasing the surface charge of the fibers and allowing for easier mechanical defibrillation. Additionally, it is well known than fibers in sodium form have greater swelling tendencies, contributing to ease

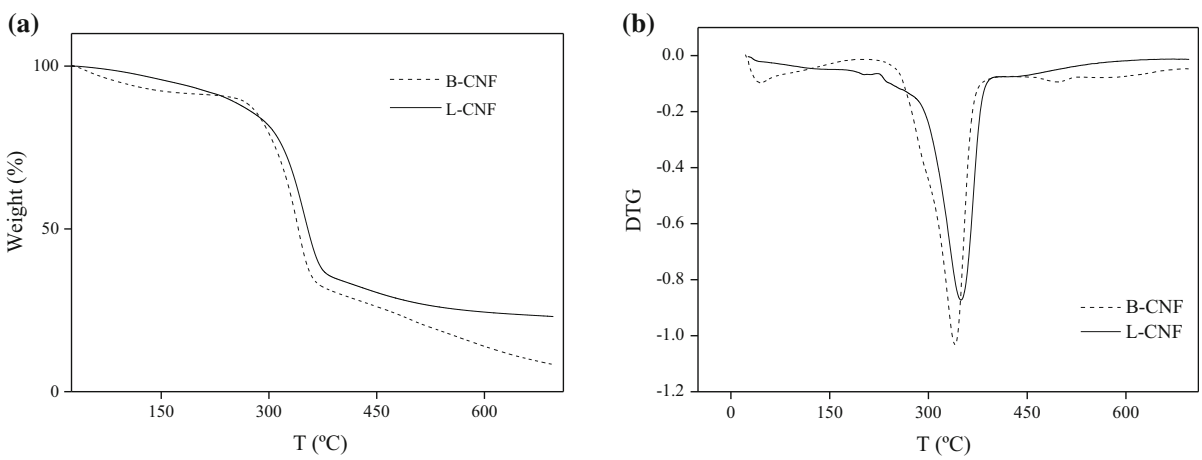

Fig. 3 Thermal stability of CNFs from **a** TGA and **b** DTG (derivative thermogravimetric analyses)

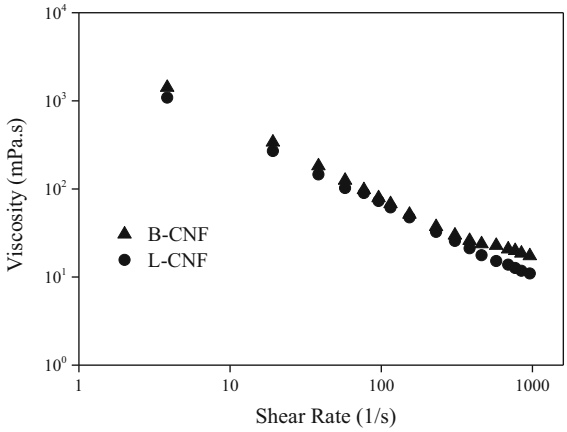

Fig. 4 Rheometric behavior of B-CNF and L-CNF suspensions

the fibrillation process (Lahtinen et al. 2014; Scallan and Grignon 1979).

The lower charge density and Z potential of the fully bleached nanofibrillated cellulose can be attributed to the loss of hemicelluloses during delignification, especially glucuronoxylans, as observed in previous studies (Ferrer et al. 2012).

Thermal behavior

Thermograms for B-CNF and L-CNF are shown in Fig. 3. CNFs exhibit a considerable thermal stability, more noticeable for L-CNF. The difference between the the two samples can be explained by the additional amount of hydrogen bonds present between cellulose, lignin, and hemicelluloses, as well as additional interactions between these components. (Wang et al. 2012). Additionally, lignin decomposes on a broader temperature range (120–500 °C) than that the other fiber constituents of native wood due to different thermal stabilities of several oxygen related to different functional groups on its structure (Brebu and Vasile 2010; Fenner and Lephardt 1981; Kim et al. 2006; Vänskä et al. 2016).

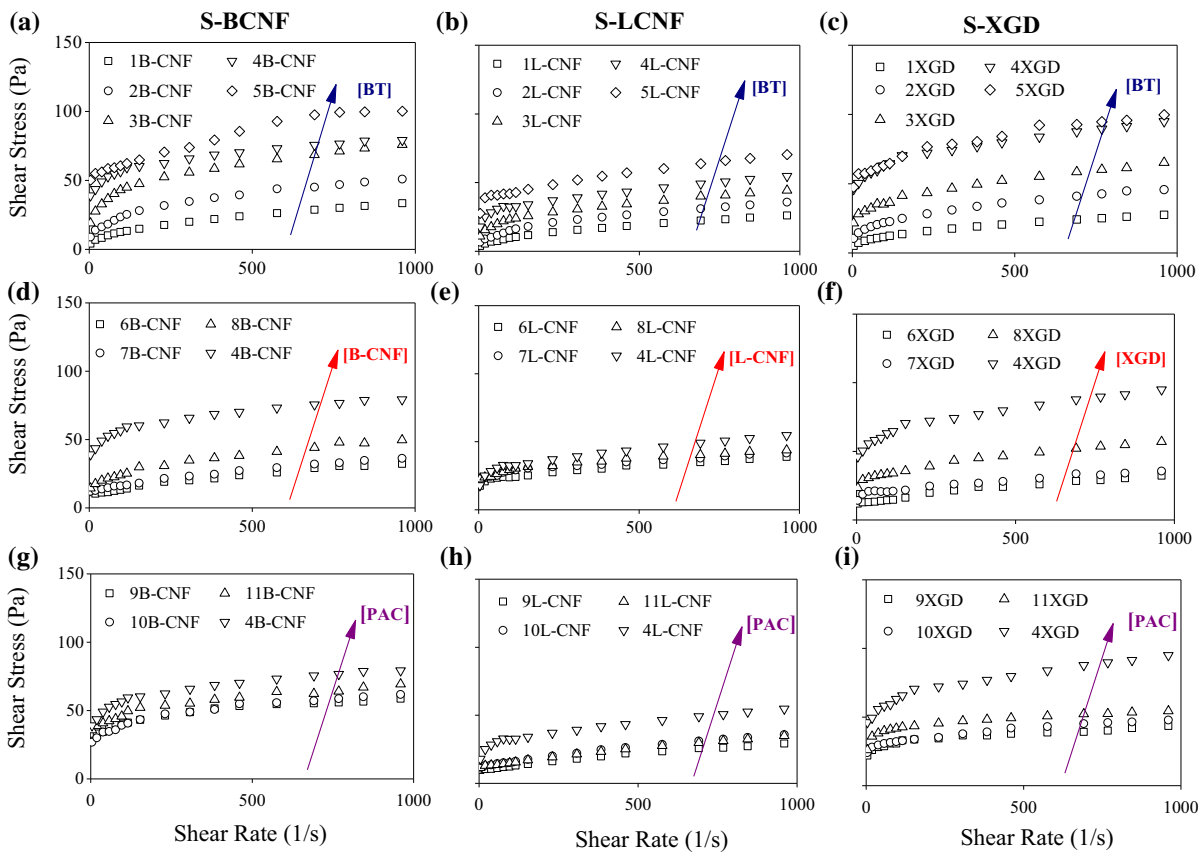

Fig. 5 Rheometric results. Effect of the concentration of: **a–c** BT; **d–f** B-CNF, L-CNF or XGD; **g–i** PAC on the studied systems

Fluids characterization

Due to the differences of dimension, shape, chemical composition and surface characteristics between the nanofibrillated cellulose samples, as well as in their rheological properties, it is expected that B-CNF and L-CNF will affect rheological and filtration properties of WBMs differently.

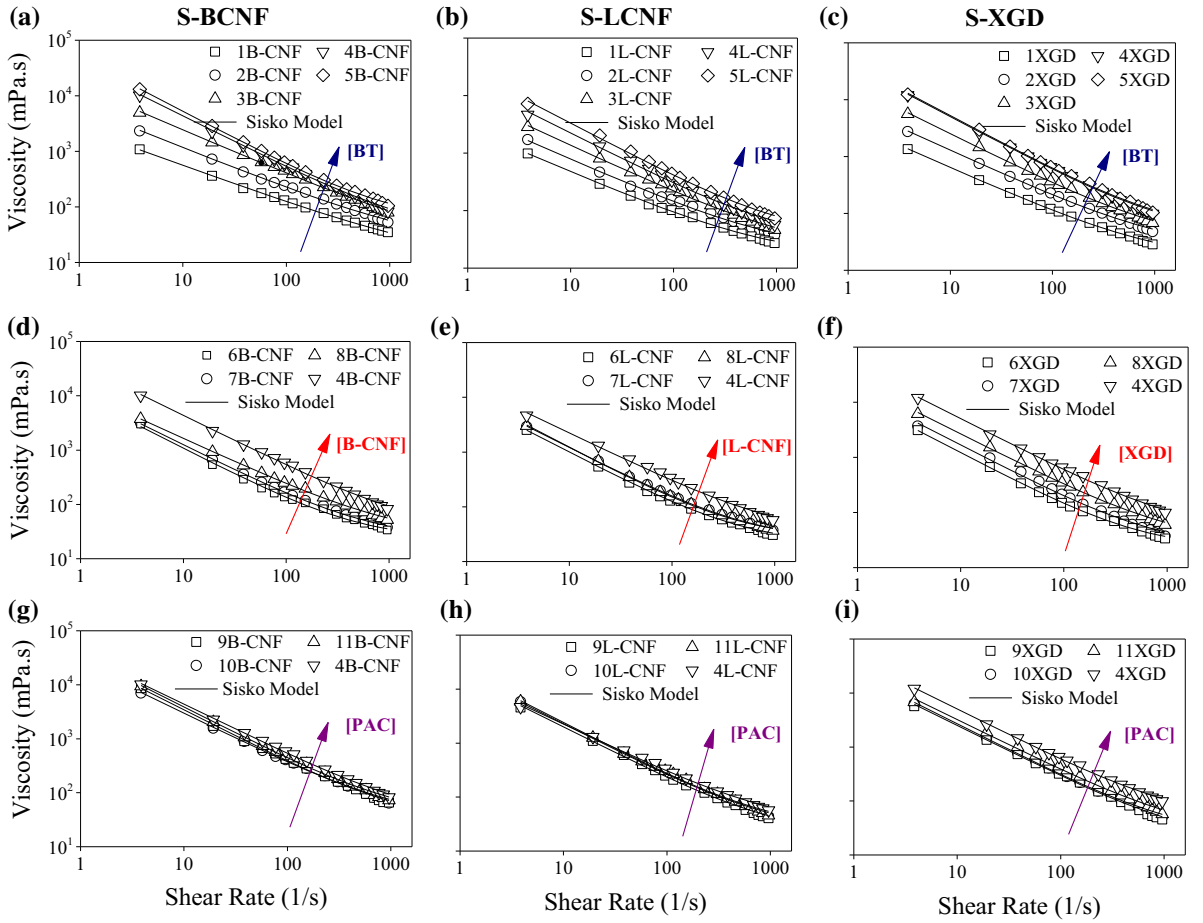

Fig. 6 Viscosity *vs* shear rate curves. Effect of the polymer concentration of: **a–c** BT; **d–f** B-CNF, L-CNF or XGD; **g–i** PAC. Simulated curves are indicated in solid lines

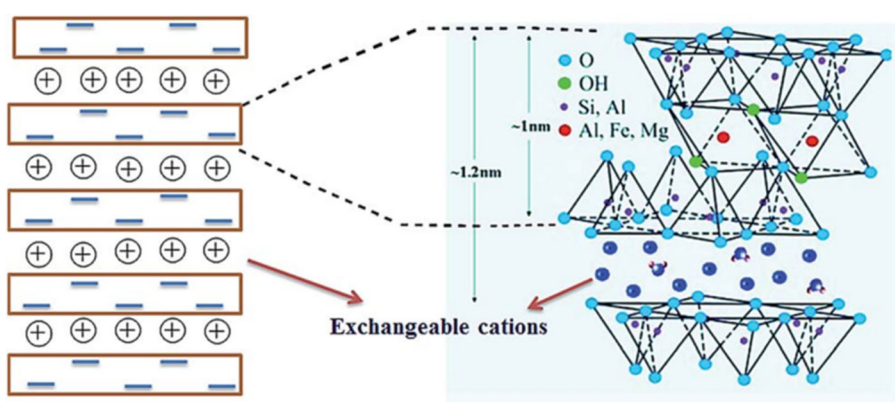

Fig. 7 Diagrammatic sketch of the structure of bentonite clay (Hebbar et al. 2014) (with permission from American Chemical Society, 2018)

WBMs results are presented in two parts. First, the effect of the composition on the rheological and filtration properties of WBMs systems (S-BCNF, S-LCNF and S-XGD) is analyzed ("Water-based drilling fluids systems" section). In the second part of this work, the effect of L-CNF on WBMs systems Argentina shale is described ("Water-based drilling fluid systems for Argentina shale" section).

Aqueous cellulose nanofibrils suspensions

Figure 4 shows the viscosity *vs* shear rate curves for CNF aqueous suspensions, both fully bleached B-CNF and unbleached L-CNF. It is observed that both nanocellulose suspensions showed a similar rheological properties. However, at greater shear rates, B-CNF exhibits greater viscosity compared with L-CNF. Such rheological properties can be explained from superficial features of CNFs, such as the greater superficial charge of L-CNF that promotes a more

Table 4 Parameters of the Sisko model for analyzed drilling fluids

System	Fluid	η_∞(mPa·s)	k(mPa·s)	n	Error (%)	R^2
S-BCNF	1B-CNF	10.06	2623.19	0.32	0.05	0.99
	2B-CNF	19.49	6457.76	0.25	0.24	0.99
	3B-CNF	23.40	15,297.56	0.20	0.32	0.96
	4B-CNF	41.07	38,239.04	0.05	0.59	0.99
	5B-CNF	57.10	49,545.11	0.02	0.17	0.99
	6B-CNF	23.14	9993.86	0.13	0.42	0.99
	7B-CNF	24.05	10,773.68	0.06	13.00	0.99
	8B-CNF	26.07	11,929.15	0.03	0.22	0.99
	9B-CNF	31.88	31,886.00	0.06	0.48	1.00
	10B-CNF	35.52	25,241.33	0.04	0.65	0.99
	11B-CNF	39.32	35,943.39	0.03	0.80	0.99
S-LCNF	1L-CNF	15.60	2707.22	0.23	0.21	0.99
	2L-CNF	20.09	4722.93	0.21	0.34	0.99
	3L-CNF	20.63	9124.88	0.17	0.46	0.99
	4L-CNF	30.48	17,606.94	0.10	0.97	0.99
	5L-CNF	35.80	28,280.87	0.06	0.49	0.99
	6L-CNF	21.63	9140.99	0.03	0.19	0.99
	7L-CNF	25.19	10,596.87	0.05	0.17	0.99
	8L-CNF	27.29	11,626.71	0.01	0.20	0.99
	9L-CNF	20.66	17,904.41	0.04	0.50	0.99
	10L-CNF	24.96	21,021.18	0.03	0.12	0.99
	11L-CNF	27.71	22,687.75	0.02	0.75	0.99
S-XGD	1XGD	15.17	3974.62	0.20	0.24	0.99
	2XGD	23.45	8461.66	0.18	0.28	0.99
	3XGD	33.67	19,636.99	0.10	0.45	0.99
	4XGD	46.72	44,667.65	0.05	0.54	0.99
	5XGD	51.09	47,082.81	0.04	0.45	0.98
	6XGD	23.18	11,390.52	0.02	0.24	0.99
	7XGD	24.66	15,248.65	0.03	0.96	0.99
	8XGD	30.74	23,103.56	0.06	0.40	0.99
	9XGD	18.65	22,033.76	0.05	0.79	0.99
	10XGD	23.82	24,402.48	0.04	0.45	0.99
	11XGD	25.44	27,548.85	0.06	1.03	0.94

stable colloidal suspension and feasibility to align under shear conditions.

Water-based drilling fluid systems

The rhelogical properties of the drilling fluids with different compositions (described in Table 1) are shown in Figs. 5 and 6. A shear thinning behavior is observed in all cases. As the concentrations of BT, B-CNF, L-CNF, XGD, and PAC increase, greater pseudoplasticity, yield stress, and viscosifier effect were observed. These effects are more noticeable in the cases of WBMs containing B-CNF and XGD. Regarding the effect of composition of B–CNF, L-CNF, or XGD, the results showed a greater viscosifier effect for the fluid containing XGD (Figs. 5d–f, 6d–f).

From the analysis of the rheometric behavior of the systems at varying PAC concentrations, the greatest impact of PAC was observed on the system with XGD (Figs. 5g–i, 6g–i). In comparison with other polymeric additives, PAC showed less effect on the viscosity of the different fluids, confirming the role of BT, B-CNF, L-CNF, and XGD as viscosifier agents.

On the other hand, when analyzing the systems containing nanocellulose (bleached and unbleached), it was observed that at the same concentration, S-BCNF exhibited greater viscosity values than the S-LCNF system. This behavior can be explained by the smaller viscosifier effect of L-CNF observed at greater shear rate values, discussed in the previous section (Fig. 4), in combination with other surface interactions occurring between CNFs and BT layers.

BT is a natural clay (Fig. 7) composed of a large number of plate-like layers with permanent negative

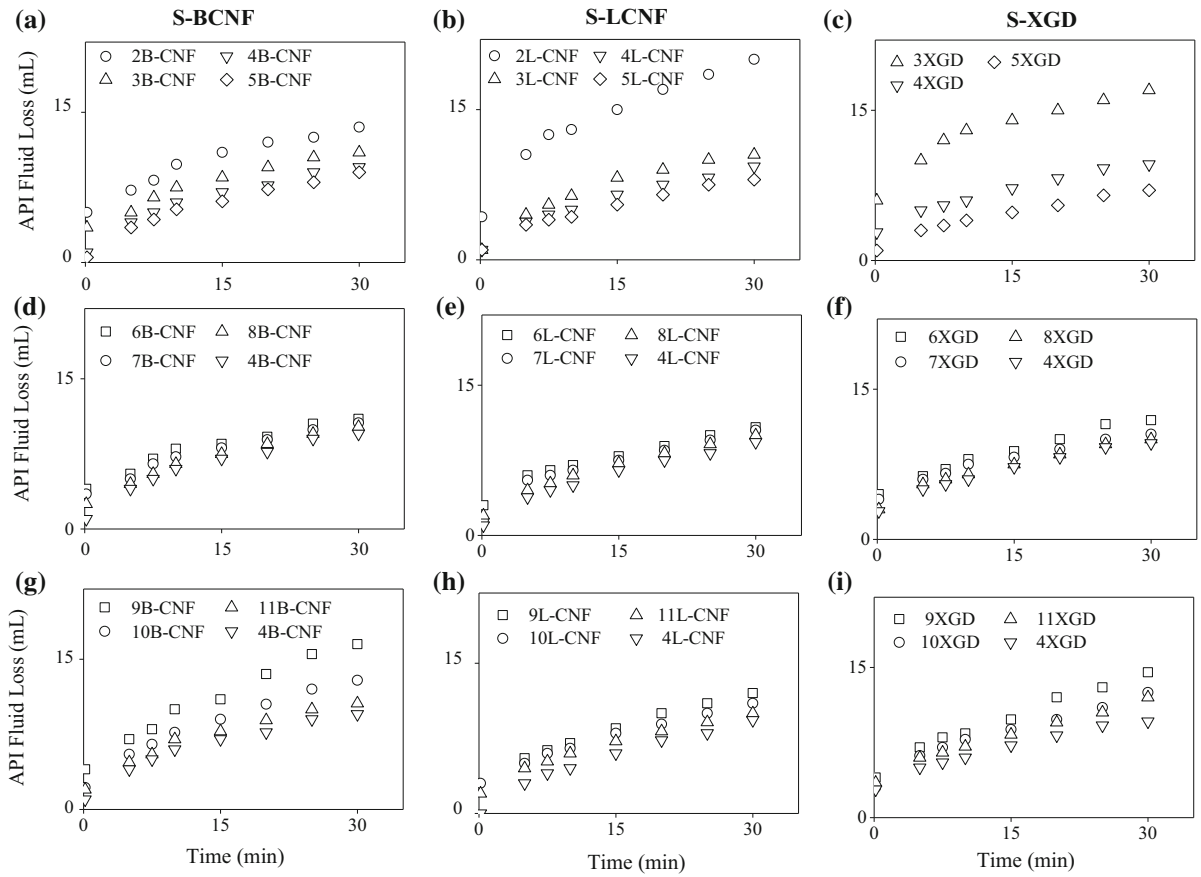

Fig. 8 API fluid loss volume *vs*. time curves for systems studied. S-BCNF (**a**, **d**, **g**); S-LCNF (**b**, **e**, **h**); and S-XGD (**c**, **f**, **i**)

charges on the flat surface and a pH-dependent charge on the edge (Jung et al. 2011; Luckham and Rossi 1999). Due to the broken bonds of the octahedral Al layers and tetrahedral Si layers on the edge, the amphoteric Al–OH and Si–OH groups are present and are conditionally charged (negative, neutral, or

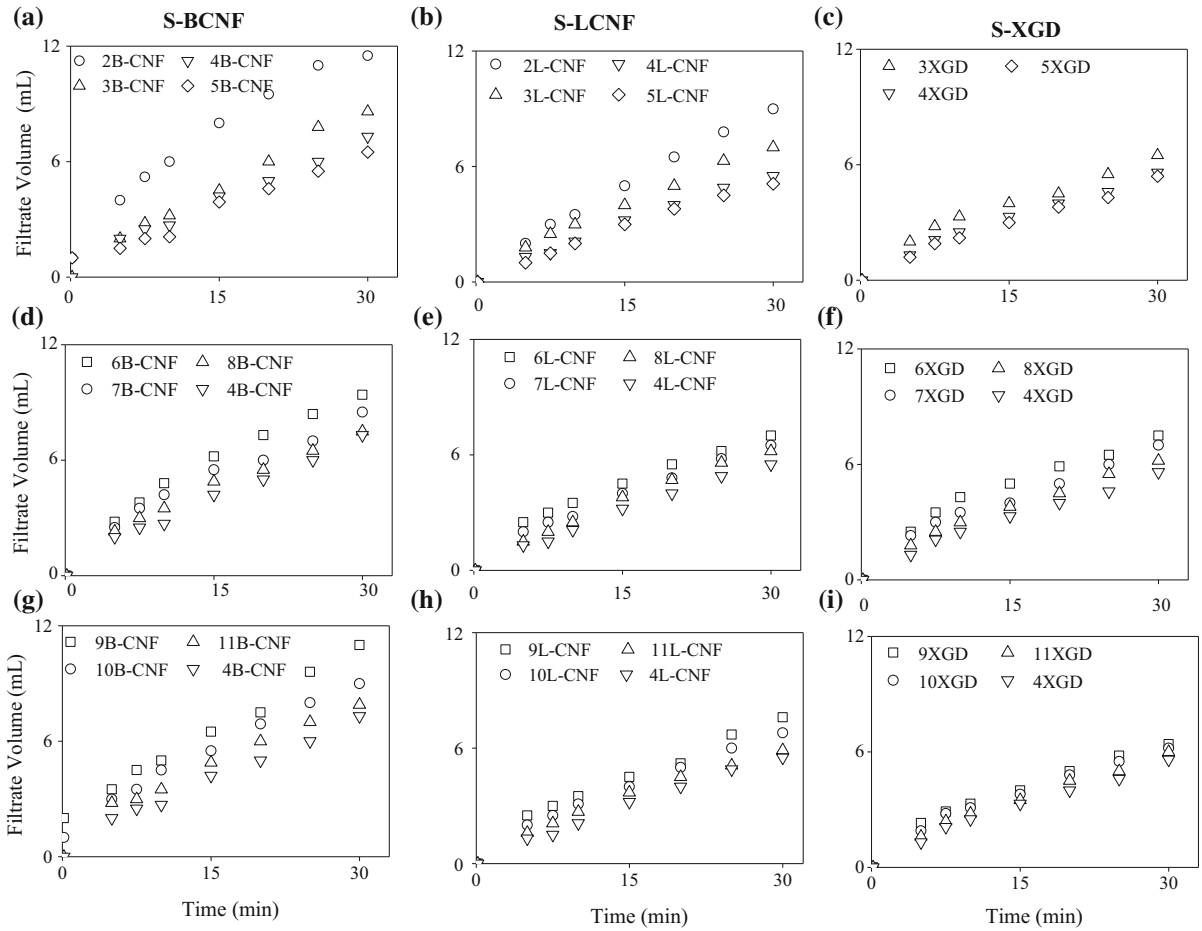

Fig. 9 Filtrate volume *vs* time curves for systems studied. S-BCNF (**a**, **d**, **g**); S-LCNF (**b**, **e**, **h**); and S-XGD (**c**, **f**, **i**)

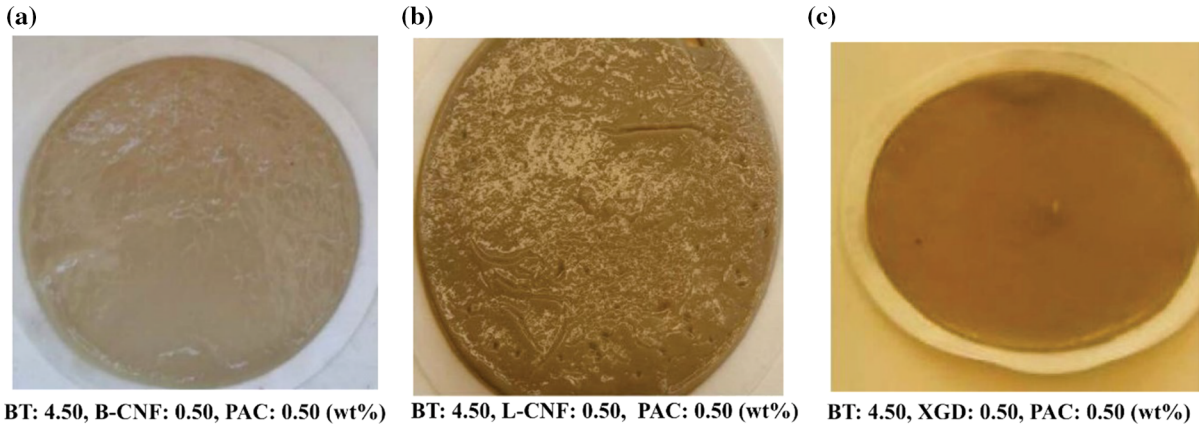

Fig. 10 Filter cakes for systems: **a** 4B-CNF; **b** 4L-CNF; and **c** 4XGD

positive). Generally, at greater pH values the edge (AlO^-) is negatively charged, at moderate pH the edge (Al–OH) is neutral, and at lower pH values the edge ($Al–OH_2^+$) is positively charged (Li et al. 2015d). However, in a neutral condition –as in the case of this work-a positively-charged edge could also be created due to the exposed octahedral Al layers. As determined previously, B-CNF is negatively charged and exhibits a stronger hydrophilic character than its counterpart lignin-containing sample (higher exposition of hydroxyl groups) (Ferrer et al. 2012; Rojo et al. 2015). When CNFs and BT are mixed in aqueous solution, CNFs could be immediately attached to the edge of BT, but at the same time some repulsive forces could be generated on the flat surface, reaching a charge balance between the two different species. Therefore, this could cause a change in the viscosity of the fluids (Darley and Gray 1988). As it has been previously shown, L-CNF particles have a greater surface negative charge, which induces greater repulsive forces with BT, and therefore a lower viscosity. Also, the negative charges of B-CNF and L–CNF promote the formation of stabilized suspensions (Morais et al. 2013).

On the other hand, because of the large number of hydroxyl groups on the surface, B-CNF has a strong gel formation capacity. Therefore, a stiff network among BT layers, B-CNF, PAC, and immobilized water molecules is created, which had a strong resistance to flow under shear force, leading to a significant increase of viscosity (Li et al. 2015d). In contrast, the presence of lignin on L-CNF decreases the amont of hydroxyl groups available on the fibril surfaces. For this reason, the surface interactions for suspensions containing L-CNF resulting from hydrogen bonds are expected to be weaker than those corresponding to B-CNF suspensions.

It is observed in Fig. 6g–i, that PAC concentration has a little effect on the viscosity of fluids. This component is a negatively-charged anionic polymer

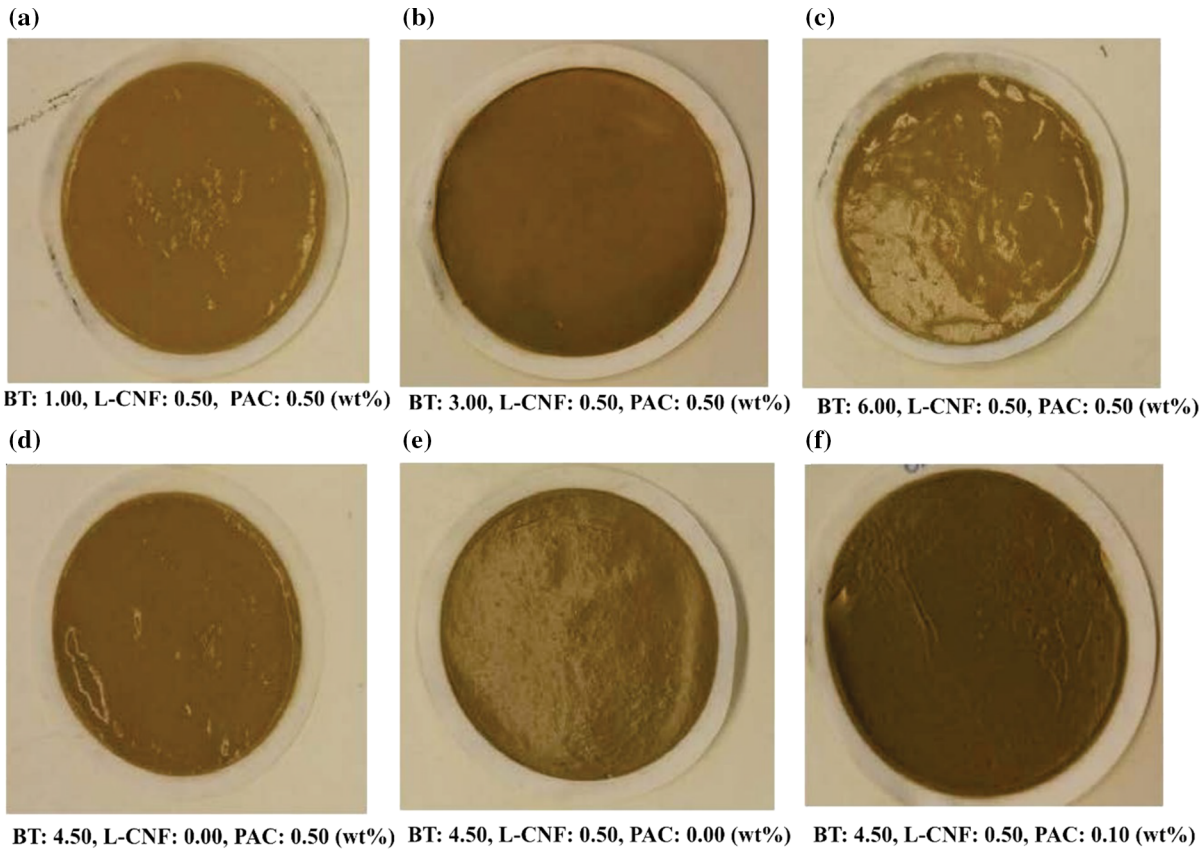

Fig. 11 Digital images of fresh filter cakes. BT/L-CNF/PAC/H_2O system: **a** 2-LCNF; **b** 3L-CNF; **c** 5L-CNF; **d** 6L-CNF; **e** 9L-CNF; and **f** 10L-CNF

due to the presence of carboxylic groups (Li et al. 2015c). Thus, when PAC is mixed with BT in an aqueous solution, it could be absorbed on the positively-charged edge of BT platelets via electrostatic attraction (Abu-Jdayil and Ghannam 2014; Warren et al. 2003). Another possible surface interaction of PAC is the formation of hydrogen bonds among them and with –OH groups of CNFs (Li et al. 2015c).

Overall, viscosity of S-BCNF and S-XGD systems are similar, which can be attributed to the similar molecular structure between B-CNF and XGD. XGD is a branched polymer of anionic nature. It superficially interacts with BT by means of electrostatic attraction in the borders of BT, and also it can form hydrogen bridges between its chains and with PAC. When XGD and PAC are mixed, a much stronger surface interaction is created in the system, leading to greater resistance of flow upon the shear force, and reflecting the continuously increased viscosity and shear stress (Fig. 6i).

Finally, it can be concluded that the rheological properties of the three analyzed systems are related to the electrostatic interactions that in term depend on the specific properties of the constituent such as molecular structure, chemical composition, morphology, and surface properties.

In order to identify the rheological properties, different models were tested and compared with the experimental results. It was found that all fluids follow the Sisko model for the studied conditions.

From the obtained experimental data, the rheological parameters of the Sisko model were adjusted using an error minimizing routine. Correlation coefficients (R^2), experimental errors, and estimated parameters are presented in Table 4. Figure 6 summarizes a comparison between the results obtained from the Sisko model and experimental data, and a good agreement between them can be observed. A non-Newtonian trend of WBMs was observed with the n parameter. Such behavior increases with BT and polymers concentration, leading to a more pronounced

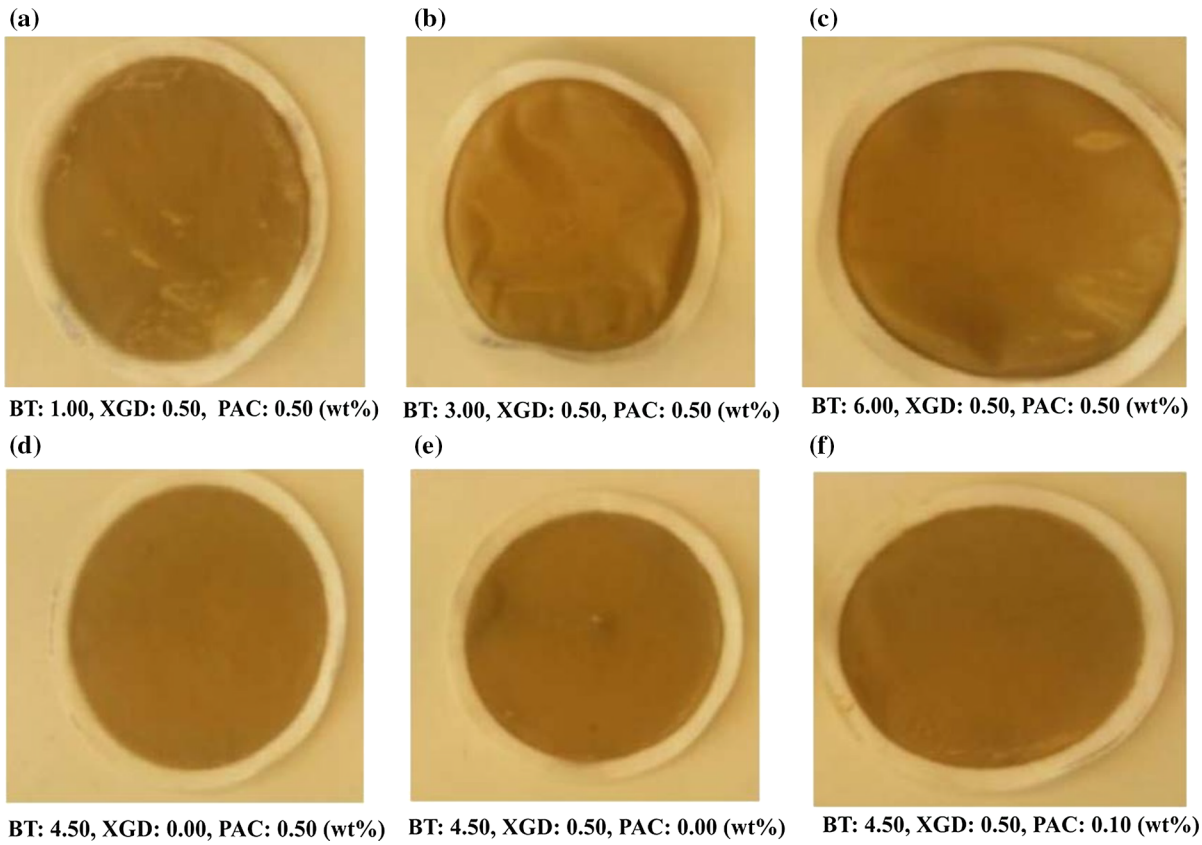

Fig. 12 Digital images of fresh filter cakes. BT/XGD/PAC/H_2O system: **a** 2XGD; **b** 3XGD; **c** 5XGD; **d** 6XGD; **e** 9XGD; and **f** 10XGD

shear thinning behavior. The greatest consistency index (k) corresponded to the systems containing XGD and B-CNF.

Filtration results for the fluids of Table 1 are presented in Figs. 8 and 9. The results show that the system with lower filtering volume corresponds to S-LCNF. As expected, the loss of fluid decreased with the increase of BT and PAC concentration, while it was slightly affected by the variation of the composition of B-CNF, L-CNF, or XGD, revealing the filter agent features of PAC. Note that the filter cakes corresponding to the BT/L-CNF/PAC/H_2O systems were more compact and dense than those obtained with the S-BCNF (Fig. 10). In addition, a similarity between S-XGD and S-LCNF cakes (Figs. 11, 12) was observed.

Results of permeability, thickness, and filtration rate are presented in Table 5. Increases of BT, B-CNF, L-CNF, XGD and PAC concentrations increased thickness and decreased filtration rate and permeability. Permeability values for S-XGD and S-LCNF systems were somewhat less than those for the S-BCNF system.

Fluids without BT or low BT concentration did not form a filter cake (1B-CNF, 1L-CNF, 1XGD and 2XGD). However, when the BT was added, fluid loss volume was reduced due to the formation of a thin compact filter cake covering the pores of the filter paper (Figs. 11, 12).

Table 5 Thickness, filtration rate, and permeability of the filter cakes

System	Fluid	t_c (cm)	$q \times 10^{-3}$ (cm^3/s)	$Kc \times 10^{-3}$ (mD)
S-BCNF	2B-CNF	0.10	5.77	1.92
	3B-CNF	0.11	4.75	1.74
	4B-CNF	0.12	3.79	1.51
	5B-CNF	0.13	3.25	1.40
	6B-CNF	0.08	4.93	1.31
	7B-CNF	0.09	4.24	1.27
	8B-CNF	0.10	3.86	1.28
	9B-CNF	0.08	4.94	1.31
	10B-CNF	0.09	4.34	1.30
	11B-CNF	0.11	4.09	1.50
S-LCNF	2L-CNF	0.09	4.91	1.47
	3L-CNF	0.11	3.77	1.40
	4L-CNF	0.13	3.08	1.33
	5L-CNF	0.14	2.87	1.29
	6L-CNF	0.09	3.56	1.07
	7L-CNF	0.10	3.42	1.14
	8L-CNF	0.11	3.33	1.22
	9L-CNF	0.09	3.86	1.15
	10L-CNF	0.10	3.58	1.19
	11L-CNF	0.11	3.14	1.15
S-XGD	3XGD	0.09	3.22	0.96
	4XGD	0.11	2.92	1.07
	5XGD	0.12	2.83	1.13
	6XGD	0.09	3.73	1.05
	7XGD	0.11	3.48	1.21
	8XGD	0.12	3.22	1.23
	9XGD	0.09	3.25	0.91
	10XGD	0.09	3.18	0.95
	11XGD	0.11	3.09	1.08

According to previous research (Li et al. 2015c), the filtration properties of drilling fluids are mainly governed by the viscosity of the fluids and the characteristics of the filter cake. In general, by increasing the fluid viscosity, filtration rates decrease. However, the best filtering properties were not obtained with a highly viscous system, suggesting that viscosity is not the only parameter to be considered, and some characteristics of the filter cake, such as permeability and microstructure, should be evaluated. In agreement with Li et al. (2015c), filtering results are related to the presence of filtering agents and the properties of filter cake (size of pores, porosity, and surface characteristics).

The difference of filtration results in S-BCNF, S-LCNF, and S-XGD can be attributed to the characteristics of the additives. The difference in results between S-BCNF and S-LCNF can be attributed to discrepancies in the size of the nanocellulose fibers and lignin content, as well as possible interactions with the medium.

In the case of S-LCNF, the lignin particles present in the L-CNF suspension act as a cement on the filter cake, reducing its porosity and therefore permeability, which is in agreement with Rojo et al. (2015). They reported that lignin acted as glue under certain conditions of temperature and pressure. Likewise, the amorphous and hydrophobic nature of lignin can serve as a seal on cake.

On the other hand, the rheological results indicated that PAC has less effect on the viscosity, it is known as a good filtering control agent. Thus, a synergistic effect is expected between L-CNF and PAC for the formation of the filter cake (Li et al. 2015d). Respect to the S-XGD system, the improvement of filtering properties is associated with the viscosifier effect of XGD, as it was observed in Villada et al. (2017).

Water-based drilling fluid systems for Argentina shale

Based on the results for the rheological and filtering properties, L-CNF was selected to be studied as a

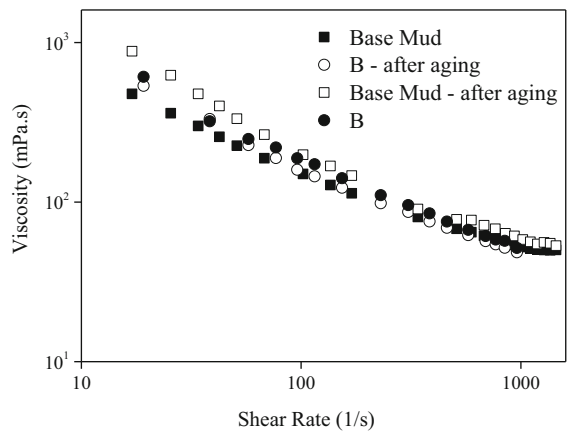

Fig. 14 Rheometrics results. Comparison between fluids without aging and aged muds

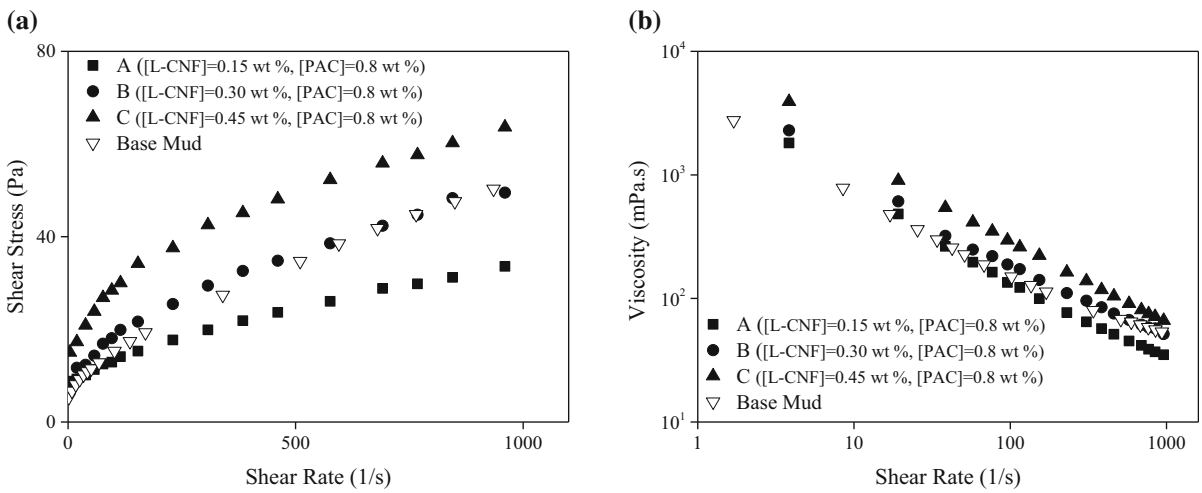

Fig. 13 Plots of **a** shear stress and **b** viscosity as a function of shear rate for WBMs for Argentina shale at various L-CNF concentrations

potential replacement of XGD in specific WBMs for Argentina shale. Three fluids with different L-CNF composition were prepared following the procedure of Villada et al. (2017) and are shown in Table 2. Note that Fluid A corresponds to the base mud containing L-CNF instead of XGD.

Rheological results of special WBMs for Argentina shale are presented in Fig. 13. The figure shows the effect of L-CNF composition on the rheological properties of WBMs. It was observed that by doubling L-CNF concentration of Fluid A, viscosities values became closer to that of base mud.

Figure 14 shows the results of the aging test applied to the base mud containing XGD and Fluid B containing L-CNF. The fluid with L-CNF (Fluid B) exhibited less variation in viscosity after aging, compared with the fluid with XGD (Base mud), and also revealed greater thermal stability.

In Fig. 15, micrographs of fluids with L-CNF obtained by SEM are shown. The effect of the L-CNF on the structure of WBM for Argentina shale

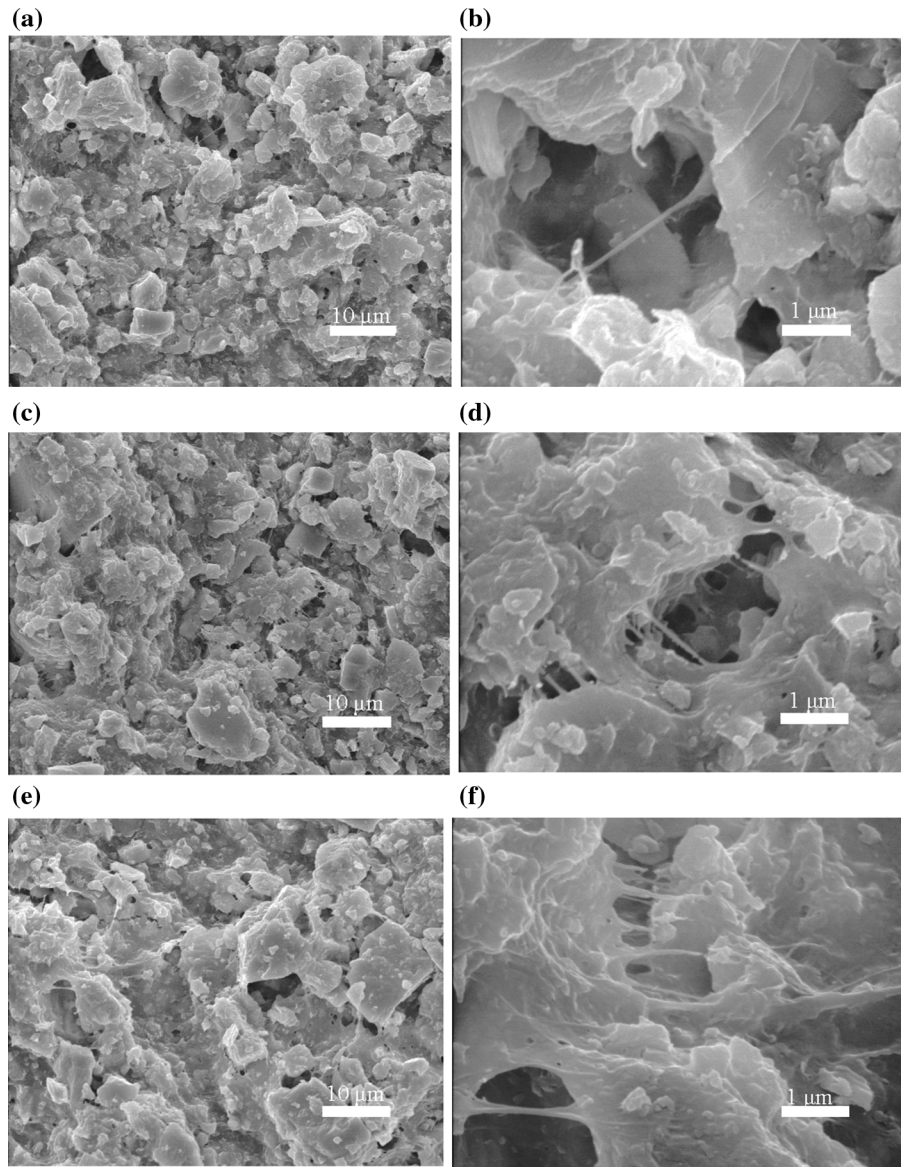

Fig. 15 Micrographs obtained by SEM. Effect of the L-CNF composition: **a**, **b** Fluid A; **c**, **d** Fluid B; **e**, **f** Fluid C

can be observed. As the concentration of L-CNF increased, a better formation of the films and greater agglomeration of the particles were noted. The tendency for the formation of films can contribute to a barrier in the filter cake, which prevents the loss of fluid towards the formation.

Conclusions

The use of CNFs with different chemical compositions, as potential replacement of XGD for drilling fluids composition was successfully studied. After measuring and comparing the different properties of both nanocelluloses, fully bleached and with remaining lignin and hemicelluloses, it can be concluded that B-CNF (bleached) could be used mainly as an additive with viscosifier characteristics in a WBMs. Alternatively, L-CNF could be more efficiently used as an additive to improve the filtering properties in the WBMs.

The system with L-CNF (BT/L-CNF/PAC/H_2O) has both rheological and filtering properties similar to the XGD system (BT/XGD/PAC/H_2O), thus L-CNF would be postulated as additive in replacement of the XGD. Additionally, L-CNF offers additional environmental and economic advantages, as it can be obtained from totally or partially unbleached lignocellulosic pulps.

Rheological parameters were obtained by following the Sisko model. The adjusted model can be used for a better optimization of the drilling fluid composition.

The set of studies performed on WBMs for Argentina shale indicated optimal rheological properties, very similar to the base mud, for systems containing L-CNF at a concentration of [L-CNF] = 0.30 wt%. In addition, such fluid presented a better thermal stability, which benefits the operational conditions.

The structural characterization of WBMs for Argentina shale indicated that the film formation and particle agglomeration were associated with the presence of polymers. This behavior tends to improve the filtration properties avoiding the loss of fluid towards the formation.

Structural differences in dimension, shape, surfaces and thermal characteristics, rheological properties, and lignin content between B-CNF and L-CNF produced different effects in the rheological and filtration properties of WBMs. Thus, changes in the viscosity, filtration volumes, thickness, permeability and filtration rate of the filter cake, and in the structure of the fluid were observed.

It was expected that the WBMs studied would exhibit viscoelastic and thixotropic properties owing to additive characteristics (Benyounes et al. 2010; Busch et al. 2018). Due to thixotropic behavior, changes in applied shear-rate can break down/build-up the microstructure of WBMs and generate changes in viscosity with time. This will be the subject of a future communication.

Acknowledgments The authors are thankful to Consejo Nacional de Investigaciones Científicas y Técnicas (CONICET), Instituto Tecnológico de Buenos Aires (ITBA) and Universidad Nacional del Litoral (UNL) for the funding. Raquel Martin Sampedro and Maria Eugenia Eugenio from the National Institute of Agricultural and Food Research and Technology (INIA, Spain) are acknowledged for providing the cellulose pulps. CNF suspensions were produced under Panu Lahtinen from VTT Technical Research Center of Finland Ltd. (Espoo, Finland) is acknowledged for producing the CNF suspensions.

References

Abu-Jdayil B, Ghannam M (2014) The modification of rheological properties of sodium bentonite-water dispersions with low viscosity CMC polymer effect. Energy Sources A 36:1037–1048

Aftab A, Ismail AR, Ibupoto ZH, Akeiber H, Malghani MGK (2017) Nanoparticles based drilling muds a solution to drill elevated temperature wells: a review. Renew Sustain Energy Rev 76:1301–1313

American Petroleum Institute (2003) Recommended practice for field testing of water-based drilling fluids, 3rd ed. American Petroleum Institute, washington, DC, p 82. ANSI/API 13B-1, 1 November 2003

Baker Hughes INTEQ (1999) FLUID facts engineering handbook. Part Number 008902097 Rev. C, December

Barry MM, Jung Y, Lee JK, Phuoc TX, Chyu MK (2015) Fluid filtration and rheological properties of nanoparticle additive and intercalated clay hybrid bentonite drilling fluids. J Pet Sci Eng 127:338–346

Benyounes K, Mellak A, Benchabane A (2010) The effect of carboxymethylcellulose and xanthan on the rheology of bentonite suspensions. Energy Sources A 32(17):1634–1643

Bian H, Chen L, Gleisner R, Dai H, Zhu JY (2017) Producing wood-based nanomaterials by rapid fractionation of wood at 80 °C using a recyclable acid hydrotrope. Green Chem 19:3370–3379

Brebu M, Vasile C (2010) Thermal degradation of lignin: a review. Cellulose Chem Technol 44:353–363

Busch A, Myrseth V, Khatibi M, Skjetne P, Hovda S, Johansen ST (2018) Rheological characterization of polyanionic cellulose solutions with application to drilling fluids and cuttings transport modeling. Appl Rheol 28:1–16

Caenn R, Chillingar GV (1996) Drilling fluids: state of the art. J Pet Sci Eng 14:221–230

Capadona JR, Van Den Berg O, Capadona LA, Schroeter M, Rowan SJ, Tyler DJ, Weder C (2007) A versatile approach for the processing of polymer nanocomposites with self-assembled nanofibre templates. Nat Nanotechnol 2:765–769

Carico RD, Bagshaw FR (1978) Description and use of polymers used in drilling, workovers, and completions. SPE Paper 7747. SPE Production technology symposium, Hobbs, New Mexico, 30–31 October

Cheraghian G, Hemmati M, Masihi M, Bazgir S (2013) An experimental investigation of the enhanced oil recovery and improved performance of drilling fluids using titanium dioxide and fumed silica nanoparticles. J Nanostruct Chem 3:78

Darley HCH, Gray GR (1988) Composition and properties of drilling and completion fluids, 6th edn. Gulf Publ Co, Houston

De France KJ, Hoare T, Cranston ED (2017) Review of hydrogels and aerogels containing nanocellulose. Chem Mater 29:4609–4631

Diop CIK, Tajvidi M, Bilodeau MA, Bousfield DW, Hunt JF (2017) Isolation of lignocellulose nanofibrils (LCNF) and application as adhesive replacement in wood composites: example of fiberboard. Cellulose 24:3037–3050

Du X, Zhang Z, Liu W, Deng Y (2017) Nanocellulose-based conductive materials and their emerging applications in energy devices-a review. Nano Energy 35:299–320

Ezell RG, Ezzat AM, Horton D (Halliburton), Partain E (The DOW Chemical Company) (2010) State of art Polymers fulfill the need for high temperature clay free drill in and completion fluids. In: AADE Paper AADE-10-DF-HO-01 conference and exhibition, Houston, Texas, 6–7 April

Fazelabdolabadi B, Khodadadi A, Sedaghatzadeh M (2014) Thermal and rheological properties improvement of drilling fluids using functionalized carbon nanotubes. Appl Nanosci 5:651–659

Fenner RA, Lephardt JO (1981) Examination of the thermal decomposition of Kraft pine lignin by Fourier transform infrared evolved gas analysis. J Agric Food Chem 29:846–849

Ferrer A, Quintana E, Filpponen I, Solala I, Vidal T, Rodríguez A, Laine J, Rojas OJ (2012) Effect of residual lignin and heteropolysaccharides in nanofibrillar cellulose and nanopaper from wood fibers. Cellulose 19:2179–2193

Gao C (2015) Potential of welan gum as mud thickener. J Pet Explor Prod Technol 5:109–112

Hamed SB, Belhadri M (2009) Rheological properties of biopolymers drilling fluids. J Pet Sci Eng 67:84–90

Hebbar RS, Isloor AM, Ismail AF (2014) Preparation and evaluation of heavy metal rejection properties of polyetherimide/porous activated bentonite clay nanocomposite membrane. RSC Adv 4:47240–47248

Herrick F, Casebier R, Hamilton J, Sandberg K (1983) Microfibrillated cellulose: morphology and accessibility. J Appl Polym Sci Appl Polym Symp 37:797–813

Horvath AE, Lindström T, Laine J (2006) On the indirect polyelectrolyte titration of cellulosic fibers. Conditions for charge stoichiometry and comparison with ESCA. Langmuir 22:824–830

Hu W, Chen S, Liu L, Ding B, Wang H (2011) Formaldehyde sensors based on nanofibrous polyethyleneimine/bacterial cellulose membranes coated quartz crystal microbalance. Sens Actuators B 157:554–559

Hubbe MA, Ferrer A, Tyagi P, Yin Y, Salas C, Pal L, Rojas OJ (2017) Nanocellulose in thin films, coatings, and plies for packaging applications: a review. BioResources 12:2143–2233

Iscan AG, Kok MV (2007) Effects of polymers and CMC concentration on rheological and fluid loss parameters of water-based drilling fluids. Energy Sources A 29:939–949

Ismail A, Aftab A, Ibupoto Z, Zolkifile N (2016) The novel approach for the enhancement of rheological properties of water-based drilling fluids by using multi-walled carbon nanotube, nanosilica and glass beads. J Pet Sci Eng 139:264–275

Jang H, Zhang K, Chon BH, Choi HJ (2015) Enhanced oil recovery performance and viscosity characteristics of polysaccharide xanthan gum solution. J Ind Eng Chem 21:741–745

Jorfi M, Roberts MN, Foster EJ, Weder C (2013) Physiologically responsive, mechanically adaptive bio-nanocomposites for biomedical applications. ACS Appl Mater Interfaces 5:1517–1526

Jung Y, Son Y, Lee J, Phuoc TX, Soong Y, Chyu MK (2011) Rheological behavior of clay a nanoparticle hybrid-added bentonite suspensions: specific role of hybrid additives on the gelation of clay-based fluids. ACS Appl Mater Interfaces 3:3515–3522

Kargarzadeh H, Mariano M, Huang J, Lin N, Ahmad I, Dufresne A, Thomas S (2017) Recent developments on nanocellulose reinforced polymer nanocomposites: a review. Polymer 132:368–393

Khodja M, Canselier JP, Cohaut N, Bergaya F (2010a) Drilling fluid technology: performances and environmental considerations. Products and Services from R&D to final solutions Igor Fuerstner, pp 227–256

Khodja M, Canselier JP, Bergaya F, Fourar K, Khodja M, Cohaut N, Benmounah A (2010b) Shale problems and water-based drilling fluid optimisation in the Hassi Messaoud Algerian oil field. Appl Clay Sci 49:383–393

Kim HS, Kim S, Kim HJ, Yang HS (2006) Thermal properties of bio-flour-filled polyolefin composites with different compatibilizing agent type and content. Thermochim Acta 451:181–188

Klemm D, Heublein B, Fink HP, Bohn A (2005) Cellulose: fascinating biopolymer and sustainable raw material. Angew Chem Int Ed 44:3358–3393

Klemm D, Kramer F, Moritz S, Lindström T, Ankerfors M, Gray D, Dorris A (2011) Nanocelluloses: a new family of nature-based materials. Angew Chem Int Ed 50:5438–5466

Kosynkin DV, Ceriotti G, Wilson KC, Lomeda JR, Scorsone JT, Patel AD, Friedheim JE, Tour JM (2011) Graphene oxide as a high-performance fluid-loss-control additive in water-based drilling fluids. ACS Appl Mater Interfaces 4:222–227

Lahtinen P, Liukkonen S, Pere J, Sneck A, Kangas H (2014) A comparative study of fibrillated fibers from different mechanical and chemical pulps. BioResources 9:2115–2127

Li M, Wu Q, Song K, Lee S, Jin C, Ren S, Lei T (2015a) Soy protein isolate as fluid loss additive in bentonite water-based drilling fluids. ACS Appl Mater Interfaces 7:24799–24809

Li MC, Wu Q, Song K, Lee S, Qing Y, Wu Y (2015b) Cellulose nanoparticles: structure-morphology-rheology relationships. ACS Sustain Chem Eng 3:821–832

Li MC, Wu Q, Song K, De Hoop CF, Lee S, Qing Y, Wu Y (2015c) Cellulose nanocrystals and polyanionic cellulose as additives in bentonite water-based drilling fluids: rheological modeling and filtration mechanisms. Ind Eng Chem Res 55:133–143

Li MC, Wu Q, Song K, Qing Y, Wu Y (2015d) Cellulose nanoparticles as modifiers for rheology and fluid loss in bentonite water-based fluids. ACS Appl Matter Interfaces. 7:5006–5016

Li MC, Wu Q, Song K, French AD, Mei C, Lei T (2018) pH-responsive water-based drilling fluids containing bentonite and chitin nanocrystals. ACS Sustain Chem Eng 6:3783–3795

Liu J, Qiu Z, Huang W (2015) Novel latex particles and aluminum complexes as potential shale stabilizers in water-based drilling fluids. J Pet Sci Eng 135:433–441

Luckham PF, Rossi S (1999) The colloidal and rheological properties of bentonite suspensions. Adv Colloid Interface Sci 82:43–92

Mahfoudhi N, Boufi S (2017) Nanocellulose as a novel nanostructured adsorbent for environmental remediation: a review. Cellulose 24:1171–1197

Mahto V, Sharma VP (2004) Rheological study of a water based oil well drilling fluid. J Pet Sci Eng 45:123–128

Mao H, Qiu Z, Shen Z, Huang W (2015) Hydrophobic associated polymer based silica nanoparticles composite with core-shell structure as a filtrate reducer for drilling fluid at ultra-high temperature. J Pet Sci Eng 129:1–14

Marchetti L, Muzzio B, Cerrutti P, Andrés SC, Califano AN (2017) Bacterial nanocellulose as novel additive in low-lipid low-sodium meat sausages. Effect on quality and stability. Food Struct 14:52–59

Menezes RR, Marques LN, Campos LA, Ferreira HS, Santana LNL, Neves GA (2010) Use of statistical design to study the influence of CMC on the rheological properties of bentonite dispersions for water-based drilling fluids. Appl Clay Sci 49:13–20

Meng X, Zhang Y, Zhou F, Chu PK (2012) Effects of carbon ash on rheological properties of water-based drilling fluids. J Pet Sci Eng 100:1–8

Moon RJ, Martini A, Nairn J, Simonsen J, Youngblood J (2011) Cellulose nanomaterials review: structure, properties and nanocomposites. Chem Soc Rev 40:3941–3994

Morais JPS, de Freitas Rosa M, de sá Moreira SF, Nascimento LD, do Nascimento DM, Cassales AR (2013) Extraction and characterization of nanocellulose structures from raw cotton linter. Carbohydr Polym 91:229–235

Nair SS, Kuo PY, Chen H, Yan N (2017) Investigating the effect of lignin on the mechanical, thermal, and barrier properties of cellulose nanofibril reinforced epoxy composite. Ind Crops Prod 100:208–217

Nakagaito AN, Yano H (2004) The effect of morphological changes from pulp fiber towards nano-scale fibrillated cellulose on the mechanical properties of high-strength plant fiber based composites. Appl Phys A 78:547–552

Nakagaito AN, Iwamoto S, Yano H (2005) Bacterial cellulose: the ultimate nano-scalar cellulose morphology for the production of high-strength composites. Appl Phys A Mater Sci Process 80:93–97

Nasser J, Jesil A, Mohiuddin T, Al Ruqeshi M, Devi G, Mohataram S (2013) Experimental investigation of drilling fluid performance as nanoparticles. World J Nano Sci Eng 3:57–61

Navarrete RC, Seheult JM, Kelco, Oil Field Group a Division of CPKelco, Coffey MD (2001) New bio-polymers for drilling, drill-in, completions, spacer and coiled tubing applications part II. SPE Paper 64982. SPE International symposium on oilfield chemistry held. Houston, Texas, 13–16 February

Navarrete RC, Himes RE, Seheult JM (2000) Applications of xanthan gum in fluid-loss control and related formation damage. SPE Paper 59535, SPE permian basin oil gas recovery conferece. Midland, Texas, 21–23 March

Ng HM, Sin LT, Bee ST, Tee TT, Rahmat AR (2017) Review of nanocellulose polymer composite characteristics and challenges. Polym Plast Technol Eng 56:687–731

Nimeskern L, Martínez Ávila H, Sundberg J, Gatenholm P, Müller R, Stok KS (2013) Mechanical evaluation of bacterial nanocellulose as an implant material for ear cartilage replacement. J Mech Behav Biomed Mater 22:12–21

Nunes RDCP, Pires RV, Lucas EF, Vianna A, Lomba R (2014) New filtrate loss controller based on poly(methyl methacrylate-co-vinyl acetate). J Appl Polym Sci 131:1–7

Olatunde AO, Usman MA, Olafadehan OA, Adeosun TA, Ufot OE (2012) Improvement of rheological properties of drilling fluids using locally based materials. Pet Coal 54:65–72

Olsson RT, Kraemer R, Lopez-Rubio A, Torres-Giner S, Ocio MJ, Lagaron JM (2010) Extraction of microfibrils from bacterial cellulose networks for electrospinning of anisotropic biohybrid fiber yarns. Macromolecules 43(9):4201–4209

O'sullivan AC (1997) Cellulose: the structure slowly unravels. Cellulose 4(3):173–207

Pääkkö M, Ankerfors M, Kosonen H, Nykänen A, Ahola S, Österberg M, Ruokolainen J, Laine J, Larsson PT, Ikkala O, Lindström T (2007) Enzymatic hydrolysis combined with mechanical shearing and high-pressure homogenization for nanoscale cellulose fibrils and strong gels. Biomacromol 8(6):1934–1941

Panshin AJ, de Zeeuw C (1970) Textbook of Wood Technology. McGraw-Hill, NY, NY, p 705

Picheth GF, Sierakowski MR, Woehl MA, Pirich CL, Schreiner WH, Pontarolo R, De Freitas RA (2014) Characterisation of ultra-thin films of oxidised bacterial cellulose for enhanced anchoring and build-up of polyelectrolyte multilayers. Colloid Polym Sci 292:97–105

Pirich CL, de Freitas RA, Woehl MA, Picheth GF, Petri DFS, Sierakowski MR (2015) Bacterial cellulose nanocrystals: impact of the sulfate content on the interaction with xyloglucan. Cellulose 22:1773–1787

Postek MT, Vladar A, Dagata J, Farkas N, Ming B, Wagner R, Raman A, Moon RJ, Sabo R, Wegner TH, Beecher J (2011)

Development of the metrology and imaging of cellulose nanocrystals. Meas Sci Technol 22:024005

Robert WA, Baker JR (1974) Use of guar gum and synthetic cellulose in oilfield stimulation fluids. In: SPE Paper 5005, 4th annual fall meeting of the society of petroleum engineers of AIME, Houston, Texas, 6–9 October

Rojo E, Peresin MS, Sampson WW, Hoeger IC, Vartiainen J, Laine J, Rojas OJ (2015) Comprehensive elucidation of the effect of residual lignin on the physical, barrier, mechanical and surface properties of nanocellulose films. Green Chem 17(3):1853–1866

Sayyadnejad M, Ghaffarian H, Saeidi M (2008) Removal of hydrogen sulfide by zinc oxide nanoparticles in drilling fluid. Int J Environ Sci Techol 5:565–569

Scallan AM, Grignon J (1979) The effect of cations on pulp and paper properties. Svensk Papperstidn 82(2):40–47

Seabra AB, Bernardes JS, Fávaro WJ, Paula AJ, Durán N (2018) Cellulose nanocrystals as carriers in medicine and their toxicities: a review. Carbohydr Polym 181:514–527

Sensoy T, Chenevert ME, Sharma MM (2009) Minimizing water invasion in shales using nanoparticles. In: SPE Paper 124429, SPE annual technical conference and exhibition. New Orleans, Louisiana, 4–7 October

Shah SN, Shanker NH, Ogugbue CC (2010) Future challenges of drilling fluids and their rheological measurements. In: AADE Paper AADE-10-DF-HO-41, conference and exhibition held at the Hilton Houston North, Houston, Texas, 6–7 April

Sharma MM, Chenevert ME, Guo Q, Ji L, Friedheim J, Zhang R (2012) A new family of nanoparticle based drilling fluids. In: SPE Paper 160045, SPE annual technical conference and exhibition. San Antonio, Texas, 8–10 October

Sjöström E (1993) Wood chemistry: fundamentals and applications, 2nd edn. Academic Press, San Diego

Solala I, Volperts A, Andersone A, Dizhbite T, Mironova-Ulmane N, Vehniäinen A, Vuorinen T (2012) Mechanoradical formation and its effects on birch kraft pulp during the preparation of nanofibrillated cellulose with Masuko refining. Holzforschung 66:477–483

Song K, Wu Q, Li M, Ren S, Dong L, Zhang X, Lei T, Kojima Y (2016a) Water-based bentonite drilling fluids modified by novel biopolymer for minimizing fluid loss and formation damage. Colloids Surf A Physicochem Eng Asp 507:58–66

Song K, Wu Q, Li MC, Wojtanowicz AK, Dong L, Zhang X, Ren S, Lei T (2016b) Performance of low solid bentonite drilling fluids modified by cellulose nanoparticles. J Nat Gas Sci Eng 34:1403–1411

Spence KL, Venditti RA, Habibi Y, Rojas OJ, Pawlak JJ (2010a) The effect of chemical composition on microfibrillar cellulose films from wood pulps: mechanical processing and physical properties. Bioresour Technol 101:5961–5968

Spence KL, Venditti RA, Rojas OJ, Habibi Y, Pawlak JJ (2010b) The effect of chemical composition on microfibrillar cellulose films from wood pulps: water interactions and physical properties for packaging applications. Cellulose 17:835–848

Spence KL, Venditti RA, Rojas OJ, Habibi Y, Pawlak JJ (2011) A comparative study of energy consumption and physical properties of microfibrillated cellulose produced by different processing methods. Cellulose 18:1097–1111

Tenhunen T, Peresin MS, Penttilä PA, Pere J, Serimaa R, Tammelin T (2014) Significance of xylan on the stability and water interactions of cellulosic nanofibrils. React Funct Polym 85:157–166

Turbak AF, Snyder FW, Sandberg KR (1983) Microfibrillated cellulose, a new cellulose product: properties, uses, and commercial potential. J Appl Polym Sci: Appl Polym Symp 37:815–827

Vänskä E, Vihelä T, Peresin MS, Vartiainen J, Hummel M, Vuorinen T (2016) Residual lignin inhibits thermal degradation of cellulosic fiber sheets. Cellulose 23:199–212

Villada Y, Gallardo F, Erdmann E, Casis N, Olivares L, Estenoz D (2017) Functional characterization on colloidal suspensions containing xanthan gum (XGD) and polyanionic cellulose (PAC) used in drilling fluids for a shale formation. Appl Clay Sci 149:59–66

Voisin H, Bergström L, Liu P, Mathew A (2017) Nanocellulose-based materials for water purification. Nanomaterials 7:57

Wang X, Cui X, Zhang L (2012) Preparation and characterization of lignin-containing nanofibrillar cellulose. Proc Environ Sci 16:125–130

Warren B, Van der Horst P, Stewart W (2003) Application of amphoteric cellulose ethers in drilling fluids. In: SPE Paper 80210, SPE international symposium on oilfield chemistry, Houston, Texas, 5–7 February

Xu X, Liu F, Jiang L, Zhu JY, Haagenson D, Wiesenborn DP (2013) Cellulose nanocrystals vs. cellulose nanofibrils: a comparative study on their microstructures and effects as polymer reinforcing agents. ACS Appl Mater Interfaces 5:2999–3009

Yan L, Wang C, Xu B, Sun J, Yue W, Yang Z (2013) Preparation of a novel amphiphilic comb-like terpolymer as viscosifying additive in low-solid drilling fluid. Mater Lett 105:232–235

Zhong H, Qiu Z, Huang W, Cao J (2012) Poly (oxypropylene)-amidoamine modified bentonite as potential shale inhibitor in water-based drilling fluids. Appl Clay Sci 67:36–43